Applied Catalysis B: Environmental 89 (2009) 365–374

Contents lists available at ScienceDirect

Applied Catalysis B: Environmental

journal homepage: www.elsevier.com/locate/apcatb

# Cobalt oxide species supported on SBA-15, KIT-5 and KIT-6 mesoporous silicas for ethyl acetate total oxidation

Tanya Tsoncheva [a,*], Ljubomira Ivanova [a], Jessica Rosenholm [b], Mika Linden [b]

[a] Institute of Organic Chemistry, BAS, Sofia, Bulgaria
[b] Center for Functional Materials, Department of Physical Chemistry, Åbo Akademi University, Porthansgatan 3-5, FI-20500 Turku, Finland

ARTICLE INFO

*Article history:*
Received 27 October 2008
Received in revised form 10 December 2008
Accepted 14 December 2008
Available online 25 December 2008

*Keywords:*
SBA-15
KIT-5
KIT-6
Mesoporous silicas
Ethyl acetate combustion
$Co_3O_4$

ABSTRACT

Cobalt oxide modified SBA-15, KIT-5 and KIT-6 mesoporous silicas with different pore size/pore entrances have been synthesized by a conventional wet impregnation method using cobalt nitrate as the precursor. The modified materials were characterized by $N_2$-physisorption, XRD, TEM-EDX, XPS, FT-IR, UV–vis and TPR-TG with hydrogen. Their catalytic activities in total oxidation of ethyl acetate were evaluated. A good correlation was observed between the catalytic activity, and the presence of spinel-type $Co_3O_4$ in the materials. Supports with larger mesopores facilitated the formation of such easily reducible spinel particles. However, the interconnectivity of the mesopores and the uniformity of the channel dimensions also had an influence on the catalytic activity, implying that mass-transfer effects, especially in the case of supports with cage-like mesopores.



## 1. Introduction

Cobalt based materials have gained a significant interest due to their high efficiency as catalysts in some important processes, such as Fischer–Tropsch (FT) synthesis [1–4], $NO_x$ removal [5,6], partial oxidation of olefins [7,8], hydrodesulfurization [9], etc. They are also considered as a suitable alternative to the high cost noble metal based catalysts for the toxic compounds elimination from the exhausted automobile and industrial emissions *via* combustion [10–17]. The efforts to improve the catalytic behaviour of these materials resulted to a deposition of cobalt on various supports, such as silica, alumina, titania, magnesia, zeolites etc., and to an intensive characterization of the state of so supported cobalt particles [9,18–20]. It has been established that the catalytic properties of such materials depend on the dispersion and interaction of the cobalt species with the support [21,22]. Generally, the relatively high cobalt dispersion leads to increasing number of catalytic active sites, but the stronger particle-support interaction in this case often reduces their activity. At the same time, the weaker interaction with the support favours cobalt oxide particle agglomeration with increasing temperature. In this respect, the preparation of cobalt species with optimal size and their stabilization under the reaction conditions is still a challenge in the heterogeneous catalysis. Many studies have been undertaken where various porous supports have been used for this purpose [23–29]. Ordered mesoporous silicas, due to their high specific surface areas, high pore volumes and narrow pore size distributions have been reported as suitable supports for various metal and metal-oxide nanoparticles [30–36]. These possibilities have been essentially expanded with the application of poly-(alkylene oxide) tri-block co-polymers as a structure-directing agent during the silica matrix synthesis. The so obtained mesoporous materials possess significantly larger pores, thicker pore walls and higher hydrothermal stability, in comparison with the analogues materials using alkylammonium-based surfactants [30,37–39]. The presence of complementary smaller, disordered micropores in the pore walls is also typical for these materials. These intra-wall pores originate from the interpenetration of the EO-portions of the surfactant into the silica network during synthesis [40–42]. It was demonstrated that the synthesis approach is very flexible, as the pore shape and interconnectivity of the silicas can be tuned in addition to the pore size by changing the template and/or the synthesis conditions used (silica/template ratio, aging temperature etc.) [43–53]. However to date, a limited number of mesoporous sieves with uniform pores, such as MCM-41 [22,28,29,26,55–60], MCM-48 [21,29,58], SBA-15 [22,24,28,54,60,27] and HMS [25] have been studied as a host matrix of cobalt oxide particles. Some data related to the preparation procedure [57,27,64,65] and pore size effect [22,25,55,61–63] on the cobalt particles dispersion, reducibility

* Corresponding author.
*E-mail address:* tsoncheva@orgchm.bas.bg (T. Tsoncheva).

0926-3373/$ – see front matter © 2008 Elsevier B.V. All rights reserved.
doi:10.1016/j.apcatb.2008.12.015

and catalytic behaviour have been reported. It was concluded that the porous structure could stabilize highly dispersed cobalt species even at higher cobalt loadings. Higher cobalt oxide dispersion was observed for mesoporous silicas with smaller pore diameters and higher surface areas. Smaller cobalt oxide particles were more difficult to reduce than larger particles, which present inside the pores of mesoporous silica. Furthermore, a higher activity and lower methane selectivity in FT synthesis was observed for cobalt species located in silicas with larger mesopores.

In the present paper we focus our attention on the effects of the pore topology on the state of supported cobalt oxide species. SBA-15 silicas with a two-dimensional (2D) hexagonal arrangement of uniform cylindrical mesopores [39,46,50], KIT-6 silicas with an *Ia***3***d* symmetry and two interpenetrating branched networks of cylindrical pores, [47,66,67] and 3D highly interconnected cage-like mesoporous silica of KIT-5 type, with a face centered cubic structure [45,49–51], are used as the supports. The pore size and pore accessibility of these silica materials were adjusted changing the silica/template ratio and aging temperature during the hydrothermal synthesis. A conventional wet impregnation method, using cobalt nitrate as a precursor, was applied for the introduction of cobalt into the silica supports. Ethyl acetate, well-known as one of the most hardly oxidized VOCs pollutants releasing in various industrial processes, is used as a probe molecule in the process of complete oxidation with molecular oxygen [68–70].

## 2. Experimental

### 2.1. Materials

SBA-15 and KIT-6 (*Ia***3***d*) silicas were prepared using Pluronic P123 triblock-co-polymer ($EO_{20}PO_{70}EO_{20}$) as structure-directing agent according to the procedures described in [46] and [47], respectively. In the case of SBA-15, a $SiO_2$/P123 molar ratio (*r*) of 60 or 75 was used. Silicas with *Fm***3***m* symmetry (KIT-5) were obtained according to the procedure described in references 48 and 49 using Pluronic F127 ($EO_{106}PO_{70}EO_{106}$) as the template. The hydrothermal treatment was varied within the temperature interval 300–420 K, and the aging time was 24 h in all cases. The templates were removed by a 30 min ethanol-HCl extraction followed by calcination with one 2 h step at 393 K and a subsequent heating rate of 1.5 K/min up to 823 K, where the sample was kept for 2 h. Generally, cobalt modifications of the template free mesoporous silicas (0.4 g) were performed by impregnation with 15 ml 0.0286 M aqueous solution of cobalt nitrate. After the impregnation, the samples were dried in rotary evaporator for 1 h at 313 K, and then at room temperature under vacuum for 3 h. The precursor was decomposed in a flow of air at 773 K for 2 h. All studied materials had a Co loading of 6 wt%. The samples were denoted as follows: Co/SBA-15(*T*,*r*), Co/KIT-6(*T*) and Co/KIT-5(*T*), where *T* was the aging temperature and *r*-$SiO_2$/P123 molar ratio.

### 2.2. Methods of investigation

Small-angle X-ray scattering (SAXS) and powder X-ray diffraction (XRD) measurements were performed using a Kratky compact small-angle system (M. Braun, Austria). The system is equipped with a position-sensitive detector (PSD 50m) consisting of 1024 channels of 55.5 μm width each. A Seifert ID-300 X-ray generator, operating at a maximum intensity of 50 kV and 40 mA, provided the Cu $K_\alpha$ radiation at λ = 1.542 Å. A Ni filter was used to remove $K_\beta$ radiation and a W filter protected the detector from the primary beam. The sample-to-detector distance was 277 mm. The sample holder was kept under vacuum during the measurements in order to minimize the background scattering from air. The $N_2$-physisorption was determined at 77 K using a Micromeritics ASAP 2010 sorptometer. The samples were outgassed at 423 K for 12 h before measurements. The specific surface area was determined using the standard BET method. Pore volumes and pore size distribution were calculated by Autosorb 1 for Windows 1.25 software (Quantachrome Instruments) using adsorption branch of the isotherms and NLDFT method. The t-plot method was used for calculating the specific micropore volumes. Transmission electron micrographs (TEM) were recorded on a Philips CM 30 ST microscope, equipped with an energy-despersive EDAX PV 9900 X-ray (EDX) unit. The FTIR spectra were recorded on a Bruker 22 spectrometer using KBr pellets at a resolution of 2.5 $cm^{-1}$ and 256 scans. The UV–vis spectra were recorded on the powder samples using a PerkinElmer Lambda 900 UV/VIS/NIR Spectrometer equipped with a diffuse reflectance unit. X-ray photoelectron spectroscopy (XPS) measurements (PerkinElmer PHI 5400 ESCA System Spectrometer) were performed at a base pressure of $1\times10^{-8}$ torr using the Mg $K_\alpha$ X-ray (*k* = 1253.6 eV) source. Adventitious carbon (284.6 eV) was used as internal standard. Sensitivity factors provided as part of the instrument software were used in the calculations. The TPR-TGA (temperature-programmed reduction-thermogravimetric analysis) investigations were performed on a Setaram TG92 instrument. Typically, 40 mg of the sample were placed in a microbalance crucible and heated in a flow of 50 vol% $H_2$ in Ar (100 $cm^3$/min) up to 873 K at 5 K/min and a final hold-up of 1 h. Prior to the TPR experiments the samples were treated in-situ in a flow of air (10 K/min) up to 773 K, followed by a hold-up of 1 h.

### 2.3. Catalytic test

The catalytic experiments were performed in a flow type reactor (0.100 g of catalyst) with a mixture of ethyl acetate (1.21 mol%) in air and WHSV-100 $h^{-1}$). Before the catalytic experiments the samples were pre-treated in air at 773 K for 2 h. Gas chromatography analyses were done on a Varian 3700 apparatus using carbon-based calibration. The products distribution is presented as $CO_2$ selectivity.

## 3. Results and discussion

### 3.1. Structural characterization

#### 3.1.1. SBA-15 materials

Small-angle X-ray diffraction patterns of parent SBA-15 materials (Fig. 1a) represent intensive well-resolved peaks, which can be indexed as the (1 0 0), (1 1 0) and (2 0 0) reflections of a 2-D hexagonal lattice with *p***6** mm symmetry (Fig. 1a) [46,53]. An increase of the unit cell parameters with the aging temperature and $SiO_2$/P123 ratio increase is observed (Table 1), in agreement with previous reports in the literature [46]. Cobalt introduction (Fig. 1b) does not alter the unit cell parameters of the SBA-15 lattice (Table 1), but leads to a significant decrease in the intensity of the reflections due to the decrease in electron density contrast [71]. In the wide-angle XRD pattern (Fig. 1b, inset) very low-intensity reflections are observed at about 37°, 59.5° and 65.5° 2θ, which correspond to the (3 1 1), (5 1 1) and (4 4 0) reflections of $Co_3O_4$ spinel phase, suggesting high cobalt dispersion in all cases.

$N_2$-physisorption isotherms of parent materials (Fig. 2a) are of type IV (IUPAC classification) with a hysteresis loop characteristic for cylindrical mesopores. A sharp capillary condensation step is registered in the relative pressure range 0.45–0.7 depending on the material, indicating the presence of uniform mesopores with a narrow pore size distribution. The specific BET surface areas, pore

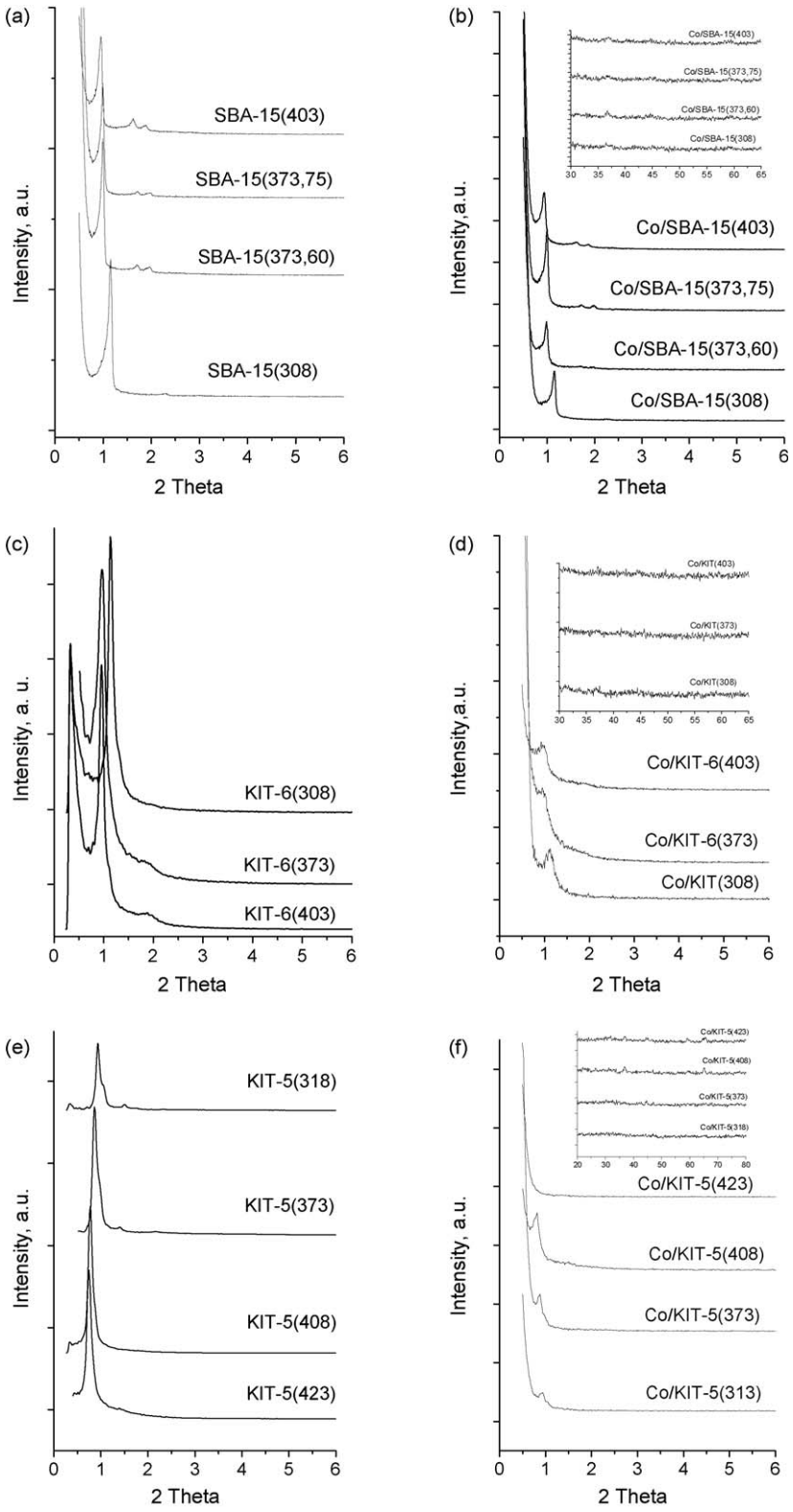


**Fig. 1.** XRD patterns of parent (a,c,e) and cobalt modified (b,d,f) silicas with different pore structure. The silicas preserve their structure after the modification. Absence or negligible reflexes typical of $Co_3O_4$ (b,d,f, inset) are registered for the cobalt modifications.

volumes (total pore volumes and micropore volumes), and mean pore diameters of the samples are listed in Table 1. After cobalt modification the adsorption isotherms exhibit almost similar features, (Fig. 2b), which is an evidence for the maintaining the structural characteristics of the silica host matrix. However, the desorption branch is not parallel to the adsorption branch after impregnation, suggesting partial pore blocking by the introduced cobalt species [72]. This feature is not evident for the Co/SBA-15(308) material, but this is due to the fact that the desorption occurs at the critical pressure of liquid nitrogen. The observed decrease in the BET surface area and pore volume (Table 1) upon impregnation is higher than what would be obtained by only

**Table 1**
Nitrogen physisorption data of parent and cobalt modified silicas.

| Sample | BET ($m^2$/g) | $V_{tot}$ (cc/g) | $V_{mic}$ (cc/g) | $D_{pores}$ (nm) | $d$ (nm) |
|---|---|---|---|---|---|
| SBA-15(308) | 431 | 0.39 | 0.04 | 4.5 | 7.6 |
| SBA-15(373,60) | 644 | 0.79 | 0.05 | 7.0 | 8.6 |
| SBA-15(373,75) | 632 | 0.69 | 0.08 | 6.2 | 8.7 |
| SBA-15(403) | 620 | 0.94 | 0.02 | 8.0 | 9.2 |
| Co/SBA-15(308) | 283 | 0.30 | 0.02 | 4.5 | 7.6 |
| Co/SBA-15(373,60) | 430 | 0.50 | 0.02 | 6.8 | 8.6 |
| Co/SBA-15(373,75) | 471 | 0.56 | 0.04 | 6.2 | 8.7 |
| Co/SBA-15(403) | 490 | 0.71 | 0.01 | 7.8 | 9.2 |
| KIT-6(308) | 359 | 0.26 | 0.09 | 5.3 | 7.7 |
| KIT-6(373) | 780 | 0.85 | 0.09 | 7.2 | 9.2 |
| KIT-6(403) | 581 | 0.66 | 0.07 | 8.1 | 9.3 |
| Co/KIT-6(308) | 207 | 0.18 | 0.03 | 5.1 | 7.7 |
| Co/KIT-6(373) | 414 | 0.38 | 0.03 | 5.0 | 9.2 |
| Co/KIT-6(403) | 432 | 0.48 | 0.03 | 8.1 | 9.3 |
| KIT-5(318) | 447 | 0.21 | 0.09 | 6.1 | 9.5 |
| KIT-5(373) | 554 | 0.36 | 0.13 | 7.6 | 10.3 |
| KIT-5(408) | 740 | 0.69 | 0.02 | 9.8 | 11.5 |
| KIT-5(423) | 562 | 0.75 | 0.00 | 9.8 | 11.7 |
| Co/KIT-5(318) | 341 | 0.15 | 0.00 | – | 9.5 |
| Co/KIT-5(373) | 345 | 0.28 | 0.06 | 9.8 | 10.3 |
| Co/KIT-5(408) | 334 | 0.39 | 0.01 | 7.7 | 11.5 |
| Co/KIT-5(423) | 455 | 0.59 | 0.00 | 8.2 | 11.7 |

BET-specific surface area, $V_{tot}$- total pore volume, $V_{mic}$- microporous pore volume, $D_{pores}$-average mesopore diameter, d- unit cell parameters ($d_{1\,0\,0}$, $d_{2\,0\,0}$ and $d_{2\,2\,0}$ for SBA-15, KIT-6 and KIT-5, respectively).

taking the mass increase upon cobalt loading into account, suggesting the presence of cobalt species inside the porous network in all cases.

### 3.1.2. KIT-6 materials

XRD patterns of parent KIT-6 materials represent two well-distinguished reflections in the small-angle region, which could be assigned to the (2 1 1) and (2 2 0) planes of 3D cubic structure (Fig. 1c) [47]. Again, a clear increase in the d-spacing with increasing aging temperature is observed (Table 1), in good agreement with literature reports [47]. After impregnation, the intensities of the reflections decrease (Fig. 2d), which could be assigned to the decrease in electron density contrast upon introduction of cobalt species into the mesopores of the silica host materials. As for the SBA-15 based materials, reflections characteristic for the spinel phase of $Co_3O_4$ are of very low-intensity in all cases (Fig. 1d, inset), suggesting a high dispersion of Co species.

Nitrogen physisorption isotherms for the parent and the cobalt-containing KIT-6 materials are shown in Fig. 2c and d, and the derived values are listed in Table 1. The isotherms are of type IV with a sharp capillary condensation step at intermediate $p/p_0$ and a hysteresis loop characteristic for materials with narrow pore size distribution (Fig. 2c). However, the tailing in the desorption branch indicates that some pores are not perfectly cylindrical. Furthermore, there is an additional hysteresis at higher partial pressures, which can be attributed to the presence of larger pores inside the particles, as the nitrogen condensing at higher relative pressure is not desorbing before the primary mesopores are emptied. The partial pore blocking effect is well pronounced for the Co-containing samples. The decrease in the BET surface area and pore volume after the cobalt introduction is more pronounced for Co/KIT-6(373), which could be assigned to higher extent of cobalt species location inside the silica pores for this material (Table 1).

### 3.1.3. KIT-5 materials

The low- and wide-angle XRD patterns measured for the KIT-5 materials are shown in Fig. 1e. The characteristic (1 1 1) and (2 0 0) reflections of a face centered close-packed cubic lattice with *Fm***3***m* symmetry are clearly resolved [49]. The pore diameters and the specific pore volumes increase with increasing aging temperature, again in good agreement with the literature [49]. The materials preserve their long-range periodic structure upon cobalt incorporation (Fig. 1f). Reflections characteristic for spinel-type $Co_3O_4$ could be observed only for Co/KIT-5(408) and Co/KIT-5(423) (Fig. 1e, inset), but also in these cases the reflections are wide and with a low-intensity, indicating the presence of small crystallites. Hence, the cage-like structure with larger pores leads to the formation of crystalline cobalt oxide particles.

Nitrogen physisorption isotherms for all parent samples are of type IV, typical of ordered mesoporous materials with cage-like pores (Fig. 2e). The hysteresis loop is much wider than those observed for the materials with cylindrical mesopores, as the desorption is delayed by the presence of smaller windows connecting the primary mesopores. The BET surface area, pore diameter and pore volume increases with increasing aging temperature (see Table 1). This is also most probably true for the window sizes, but due to the fact that desorption occurs at the critical pressure for nitrogen for all KIT-5 materials studied apart from KIT-5(423), estimation of the pore window sizes cannot be made in these cases. This holds true also for the Co-containing samples. It should be stressed that the mesopore volume practically vanishes for the KIT-5(318) sample upon impregnation.

TEM images of selected cobalt modified materials are presented in Fig. 3. A well-resolved contrast, characteristic of certain silica mesopore structure symmetry, is still observed, which is an indication for the preservation of the long ordered arrangement of the channels in the silica host matrix after the cobalt deposition. The places with darker contrast could be assigned to the presence of cobalt oxide particles with different dispersion. This assumption is confirmed by EDX data, where the estimated Co/Si atomic ratio was usually about 0.062–0.087 and well correlates with the loaded cobalt amount. The small dark spots in the images could be ascribed to cobalt oxide particles, probably located into the support channels. The larger dark areas over the channels most likely correspond to cobalt agglomerates on the external surface. Their appearance is not surprising and it is in a good agreement with the data reported in [63], where a migration of the cobalt species to the outside of the support during the calcination procedure was observed. However due to the low contrast in the images, more quantitative conclusions could not be drawn.

### 3.2. Spectroscopic characterization

The FT-IR spectra for Co/KIT-5 samples are shown in Fig. 4, and the spectra measured for the other Co-containing samples are given in the ESI. Both spectra of parent and cobalt modified silicas exhibit intensive absorption bands at 1080, 1250 and 800 $cm^{-1}$, which arise from the silica host matrix [73–79]. The band at around 960 $cm^{-1}$ could arise both from Si–OH and Si–O- stretching vibrations [77,78]. Here, a simultaneous slight shifting of the bands at around 960 and 1080 $cm^{-1}$ is observed in some cases after cobalt modification. Some authors assigned these features to the existence of strong interaction between the silica support and the loaded cobalt oxide species [75]. However, in our case the spectral resolution is not high enough to allow a detailed analysis of this effect. Two additional bands at about 680 and 560 $cm^{-1}$, appearing only in the spectra of the cobalt loaded materials, originate from the stretching vibrations of the metal-oxide bond in the $Co_3O_4$ spinel lattice [76]. The band at around 580 $cm^{-1}$ is associated with the $BOB_3$ vibrations in the spinel latice, where **B** denotes the Co ions in octahedral position, i.e. $Co^{3+}$. The second

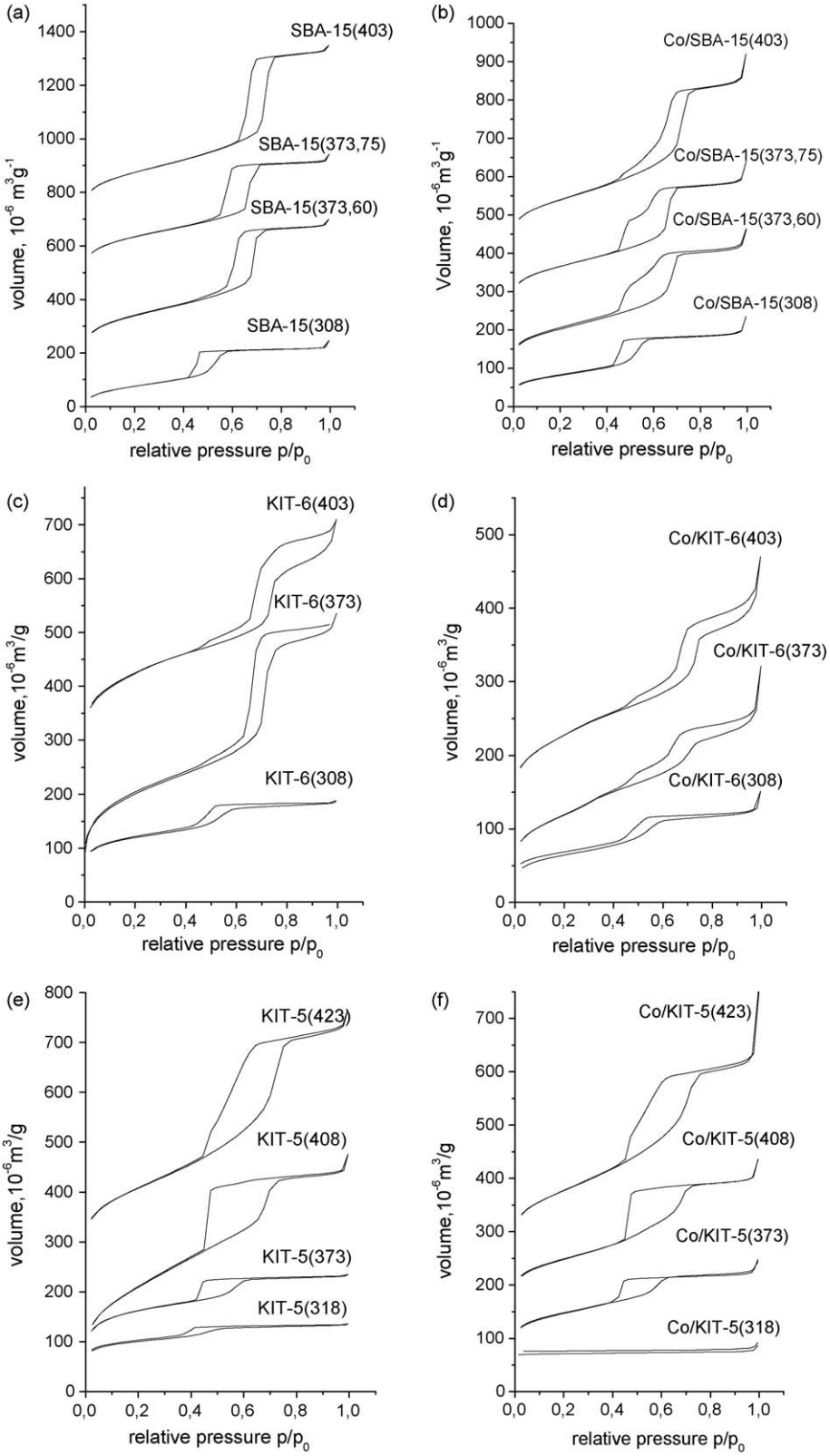


**Fig. 2.** Nitrogen physisorption isotherms of parent (a,c,e) and cobalt modified (b,d,f) silicas.

band at around 667 $cm^{-1}$ is attributed to $ABO_3$ vibrations, where **A** denotes the metal ions in tetrahedral position. The intensities of these bands increase with increasing aging temperature during the silica synthesis, i.e. for increasing mesopore size, indicating the facilitated formation of spinel-type $Co_3O_4$ particles in these cases. This holds true also for the KIT-6 materials (see ESI). For the SBA-15 supported materials, the most developed spinel structure is observed for Co/SBA-15(373,75) and Co/SBA-15(403).

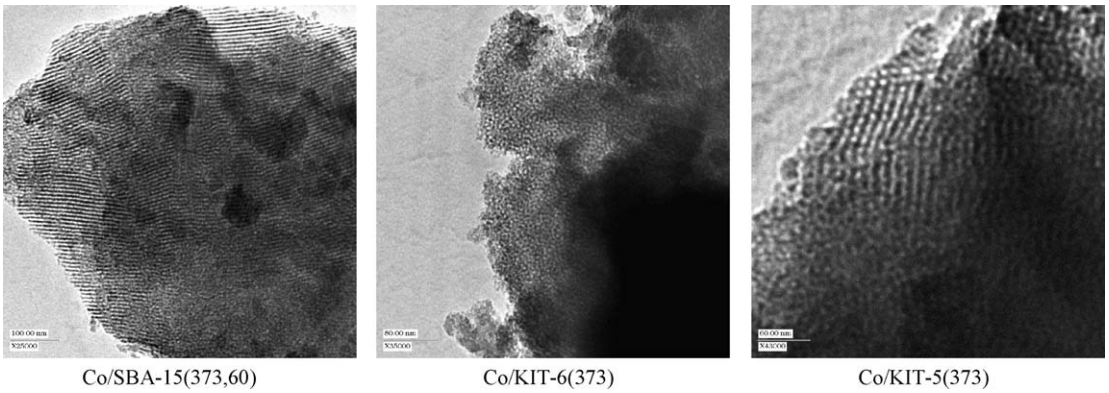


**Fig. 3.** TEM images of selected cobalt modifications. The preservation of the silica structure is observed after the cobalt oxide loading.

UV–vis spectra of selected cobalt modifications are shown in Fig. 5. Some authors reveal that the features of the spectra are closely related to the degree of crystallinity of the supported cobalt oxide particles [80,81]. The coexistence of various cobalt oxide species, formed during the decomposition of nitrate precursor, was discussed in [82]. According to these considerations, the broad peaks at about 400 and 700 nm in the spectra (Fig. 5) could be assigned to $Co^{3+}$ ions in octahedral environment from well-ordered $Co_3O_4$ species [83,84]. The wide bands at 538 and 640 nm are commonly ascribed to the ligand field $^4A_2(F) \rightarrow {}^4T_1(P)$ transition of $Co^{2+}$ ions in tetrahedral coordination [29,85]. According to [80] they could be included in amorphous cobalt oxide clusters, strongly interacting with the silica support. Thus, the spectra indicate the formation of $Co_3O_4$ particles with different degree of dispersion, which are in different interaction with the support. More information for their distribution is obtained by TPR measurements (see. Section 3.3).

XPS atomic percents of O1s, Si2p and Co2p species for all cobalt modifications are listed in Table 2. It is known, that the XPS spectra predominantly reflects the composition of the surface region, and the ratio between the Co2p and Si2p atomic percents could provide information for the dispersion of the Co species on the silica surface [86]. For the SBA-15 based materials (Table 2), this ratio passes through the maximum with the aging temperature increase and decreases with the $SiO_2$/P123 ratio change from 60 to 75. The increased surface Co dispersion for the samples aged up to 373 K could be due to the increased BET surface area of the corresponding silica supports. The decrease in the surface cobalt concentration for the sample aged at the highest temperature, Co/SBA-15(403), could be due to the facilitated cobalt species migration and agglomeration through the larger pores of the silica matrix. Almost the same could be the reason for the decreased dispersion for Co/SBA-15(373,75), where the microporosity is most pronounced. For the KIT-5 and KIT-6 based materials, a well-defined effect of a decrease in the surface cobalt concentration with the increase in the porous volume and pore diameter/entrances is observed. Here

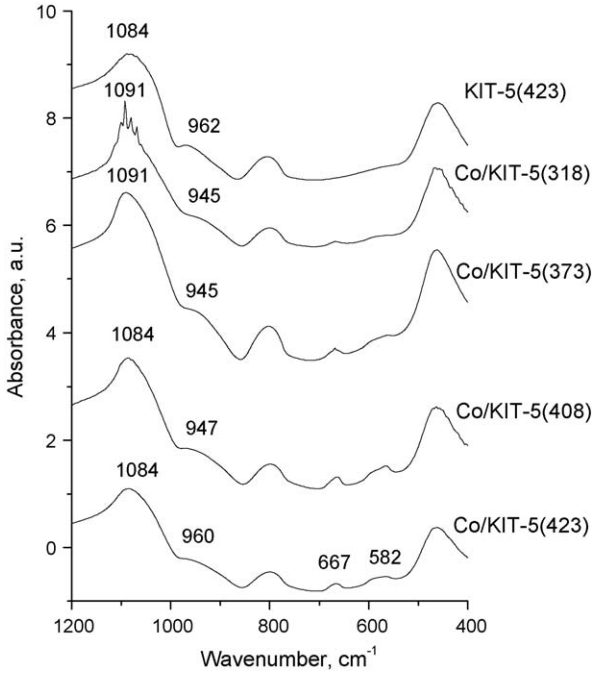


**Fig. 4.** FTIR spectra of selected parent and cobalt modified materials. Presence of cobalt oxide species with different degree of crystallinity and different interaction with the silica support could be assumed.

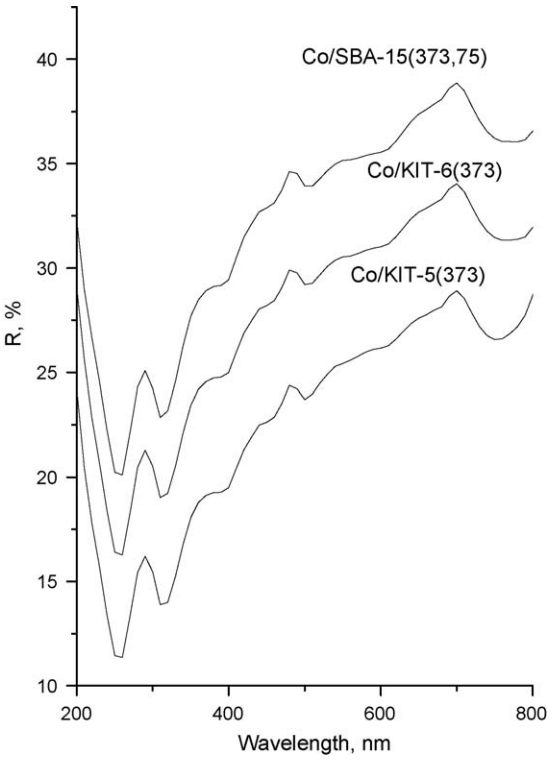


**Fig. 5.** UV–vis spectra of selected cobalt modifications. Presence of cobalt oxide species with different degree of crystallinity could be assumed.

**Table 2**
XPS atomic percents of O1s, Si2p and Co2p species, Co/Si atomic ratio and total reduction degree ($X_{TPR}$%) for cobalt modified silicas.

| Sample | O1s | Si2p | Co2p | Co/Si | $X_{TPR}$% |
|---|---|---|---|---|---|
| Co/SBA-15(308) | 72.29 | 26.53 | 1.24 | 0.047 | 78.70 |
| Co/SBA-15(373,60) | 73.39 | 24.52 | 2.09 | 0.085 | 100.00 |
| Co/SBA-15(373,75) | 73.45 | 25.57 | 0.97 | 0.038 | 80.16 |
| Co/SBA-15(403) | 73.88 | 25.66 | 0.45 | 0.017 | 88.48 |
| Co/KIT-6(308) | 74.01 | 24.37 | 1.62 | 0.066 | 26.42 |
| Co/KIT-6(373) | 74.52 | 24.39 | 1.09 | 0.045 | 90.52 |
| Co/KIT-6(403) | 74.44 | 24.79 | 0.74 | 0.029 | 65.81 |
| Co/KIT-5(318) | 72.23 | 26.01 | 1.76 | 0.067 | 36.70 |
| Co/KIT-5(373) | 73.67 | 24.59 | 1.73 | 0.070 | 51.27 |
| Co/KIT-5(408) | 71.77 | 27.24 | 0.97 | 0.036 | 80.40 |
| Co/KIT-5(423) | 70.80 | 28.82 | 0.38 | 0.013 | 55.82 |

again, the intensive processes of migration and agglomeration of the loosely interacted with the silica cobalt oxide species within the well-organized porous structure could be a reason for the observed effect. This assumption well correlates with the XRD measurements, where the formation of $Co_3O_4$ phase is registered for these samples (see above).

Another possible reason for the observed decrease in the Co/Si surface ratio is the facilitated location of the cobalt species deep into the porous matrix [87] that is mainly observed for the silicas with well-developed porous structure and larger pore diameters or pore entrances. In this respect, the observed Co/Si ratio decreases with increasing pore diameter (and pore volume) of the support, which was observed for the given structure, could be understood as more homogeneous dispersion of cobalt species in the silica supports with larger pore diameters. However, the calculated Co/Si atomic ratio (corresponding to 6 wt% loaded Co) is 0.064, which is higher than experimentally observed one for most supports with larger mesopores. Moreover, for the supports with smaller mesopores and for the Co/SBA-15(373,60) material, the values are slightly higher than the calculated one, which suggests that the impregnation efficiency was lower in these cases. We note, however, that quantitative XPS surface analysis can be complicated if particles with diameters larger than the escape length of photoelectrons (about 5 nm) are present on the outer surface, and that the corresponding value for mesoporous silica with empty mesopores is bound to be higher. However, the trend in the data is clear and can serve for further discussion.

### 3.3. TPR-TG study

TPR-DTG profiles measured for the studied materials are presented in Fig. 6. They exhibit three well resolved peaks with maxima centered at around 520–545 K, 613–685 K and 820–860 K. However, the total reduction degree remained well below 100% in most cases (Table 2). It is known that unsupported bulk $Co_3O_4$ oxide would be completely reduced already at 750 K, smaller particles being more easily reducible than larger ones in this case [19,24,88]. However, supported cobalt oxide particles show a different reduction behaviour in comparison with unsupported ones ([22,25,28,22,89,90] and refs. therein). The interpretation of the TPR-DTG profile in this case is therefore rather complicated due to its dependency on the degree of dispersion of the loaded particles, resulting in different relative influence of the interaction with the support [24,25,84]. According to literature data [21,22,24,88], the two peaks in the 520–685 K region can be ascribed to the step-wise reduction of $Co_3O_4$ crystalline particles to CoO, and then to metallic Co. Some authors suggest that the position of the first peak is not significantly influenced by the $Co_3O_4$ dispersion, and that the particle size effect is typical only for the second stage of CoO reduction to metal [22,61,62]. They concluded that for the supported materials, larger particles are reduced more easily, giving more intensive reduction peaks in the 600–700 K region in comparison with smaller particles. Typically, the TPR-DTG effects above 800 K, i.e. the fraction of particles not being reduced under our experimental conditions, are related to the reduction of significantly smaller cobalt oxide species in strong interaction with the support [21,89–92].

Thus, the co-existence of three types of $Co_3O_4$ particles could be assumed for all cobalt modified SBA-15, KIT-5 and KIT-6 materials (Fig. 6, Table 2). The first type (a) are easily reducible, relatively larger species, loosely interacting with the support; the second type (b) represents hardly reducible and well-dispersed fraction in moderate interaction with the silica, and finally, particles of type (c) are very finely dispersed, strongly interacting with the support, which could not be reduced up to 873 K. According to [67,89], these Co species could be included in various silicate- or hydrosilicate-structures. The TPR profiles are very similar for all studied Co/SBA-15 materials, which reveals a minor pore size effect on the state of the cobalt species in this series. Generally, the presence of almost uniform, easily reducible particles could be considered for these materials (Fig. 6a). This assumption is

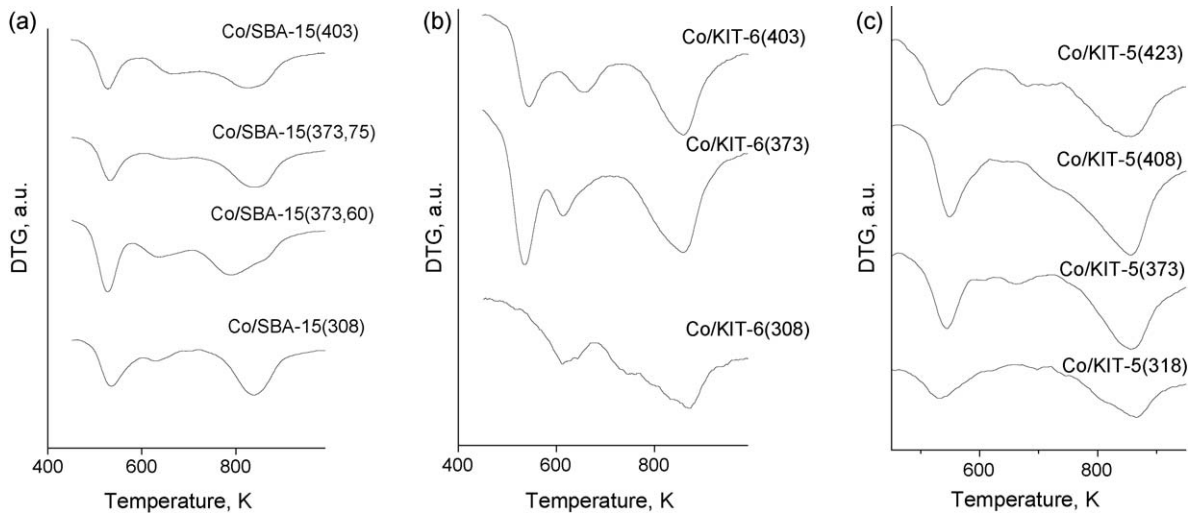


**Fig. 6.** TPR profiles for cobalt modified SBA-15 (a), KIT-6 (b) and KIT-5 (c) silicas with different pore size/entrances. Presence of cobalt oxide species with different size and interaction with the support could be concluded.

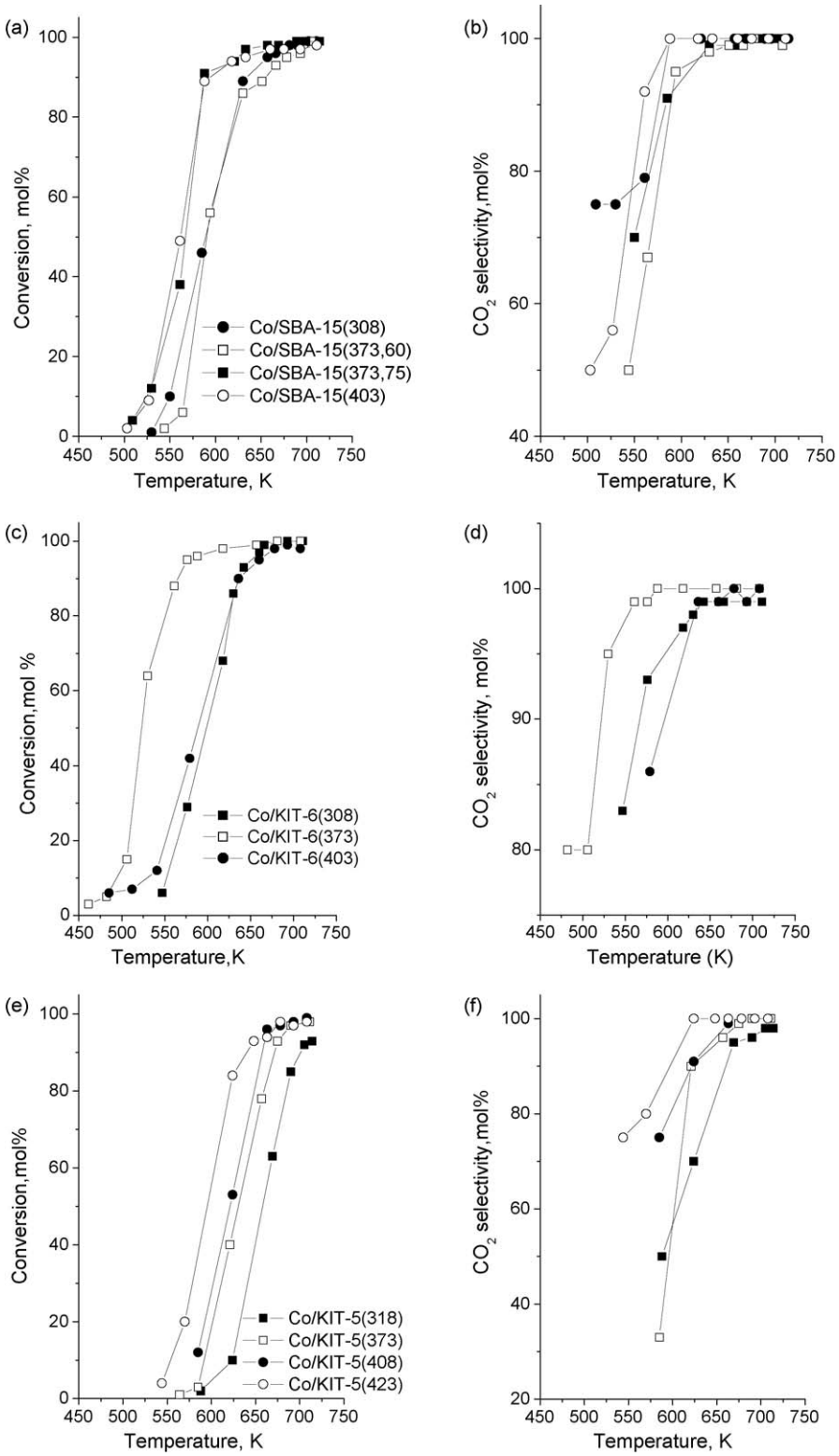


**Fig. 7.** Temperature dependencies of ethylacetate conversion (a,c,e) and $CO_2$ selectivity (b,d,f) for cobalt modified silicas with different pore topology.

supported by the relatively low temperatures of cobalt reduction as well as by the high total reduction degrees (80–100%). However, the presence of a significant amount of amorphous, cobalt oxide species strongly interacting with the silica, i.e. types (b) and (c), could be assumed for the material with the smallest pore volume and pore diameter, Co/SBA-15(308), as well as for the sample with a higher degree of microporosity, Co/SBA-15(373,75). Most inhomogeneously dispersed particles with close fractions of relatively large (type a) and strongly interacting with the support species (b and c types) could be assumed for Co/SBA-15(403). However, as stated above, overall the differences in the TPR responses of the Co/SBA-15 materials are small.

Much pronounced differences were observed the Co/KIT-6 materials (Fig. 6b, Table 2). Among the samples of this series, Co/

KIT-6(373) exhibited the highest intensity of the second peak, which is centered at relatively lower temperatures. According to [22] this can be attributed to the presence of a significant portion of crystalline species weakly interacting with the support. This assumption is also confirmed by the highest total reduction degree (above 90%), which is observed in this case. For the KIT-6(403) sample, both low temperature reduction peaks are broader and could be ascribed to the presence of more inhomogeneously dispersed cobalt oxide particles, which are not completely reduced to metallic cobalt in the temperature interval 500–750 K. The TPR profile of Co/KIT-6(308) differs significantly from that of the other materials. It exhibits much broader reduction peaks, which are shifted towards higher temperatures and a significantly lower total reduction degree (below 30%). We ascribe these observations to the presence of amorphous, hardly disordered cobalt oxide species (types b, and mainly c), strongly interacting with the support, and this assumption well correlates with XRD and FTIR data, where no peaks typical of cobalt spinel lattice were observed (Figs. 1 and 4). We could assume that the smallest pore size of this silica matrix restrict the agglomeration of the cobalt particles in them. It is not excluded also the lower reduction degree to be due to the presence of much larger cobalt oxide particles, located on the outer surface but we have not strong evidence for their formation judging from the XRD and FTIR data (see above). Similar assumption could be done for the Co/KIT-5(318) sample (Fig. 6c, Table 2), which exhibits reductive effects mainly in the high temperature region with a very low degree of reducibility (about 37%), typical of species types c. On the contrary, much higher reducibility is established for the samples with larger pores, but similarly to the channel-like structures, the reducibility passes through a maximum, depending on the size of the pore entrances (Table 2), being the highest for the Co/KIT-5(408) material. Here again, the data from the TPR-DTG analysis are in a good correlation with the FTIR measurements, supporting facilitated formation of spinel-type $Co_3O_4$ species in the case of silicas with larger mesopores.

### 3.4. Catalytic study

In Fig. 7 are shown data for the catalytic activity and selectivity to $CO_2$ in ethyl acetate (EA) oxidation for different cobalt modified mesoporous silicas. The catalytic activity of all materials strongly increases in the 500–600 K region. At lower degree of conversion, ethanol, acetaldehyde and acetic acid are also registered as products of EA partial oxidation. For the SBA-15 based materials (Fig. 7a and b) synthesized with one and the same $SiO_2$/P123 ratio (60), the sample with the largest mesopores, Co/SBA-15(403), exhibits the best catalytic activity, while practically no pore size effect could be seen for the Co/SBA-15(373,60) and Co/SBA-15(308) samples. For the samples aged at the same temperature, the material synthesized using a higher $SiO_2$/P123 ratio (75) exhibits a higher catalytic activity. So, the main observation is that the highest catalytic activity is observed for materials containing larger spinel $Co_3O_4$ species (see Figs. 1 and 6, Table 2 and FTIR spectra in ESI), well-distributed inside the silica matrix (Table 2, XPS data), as generally is the case for supports with larger mesopores. The lowest catalytic activities in the SBA-15 series are thus observed for Co/SBA-15(308) and Co/SBA-15(373,60), which contain a large fraction of amorphous cobalt oxide species and with a larger fraction of cobalt species being located outside the mesopore network (see Fig. 1, and FTIR spectra in ESI). Easier mass-transfer inside materials with larger mesopores as compared to supports with smaller mesopores could also contribute to enhanced catalytic activity.

For the KIT-6 modifications (Fig. 7c and d), the best catalytic activity is achieved for Co/KIT-6(373), where easier reducibility (Fig. 6, Table 2) of almost homogeneously dispersed (Table 2), well-crystallized (FTIR spectra in ESI) $Co_3O_4$ species were demonstrated. On the contrary, the materials with lower degree of reducibility, Co/KIT-6(308) and Co/KIT-6(403), exhibit significantly lower catalytic activity. It could be both due to the presence of amorphous cobalt oxide particles, which are in strong interaction with the silica support, as well as due to the formation of much larger particles mainly situated on the outer surface in the case of Co/KIT-6(308) or the formation of larger spinel-type $Co_3O_4$ particles inside the pores of Co/KIT-6(403) which in this case could lead to a lower effective concentration of active sites in this material.

For the materials of series KIT-5 (Fig. 7e and f) a well-defined trend of the catalytic activity increase with the increasing mesopore diameter was observed, which again is in a good correlation with the formation of relatively well-crystallized (Figs. 2 and 4) and highly reducible (Fig. 6, Table 2) cobalt oxide particles. Note the lower reducibility combined with higher activity for Co/KIT-5(423) in comparison with Co/KIT-5(408), which could be ascribed to the facilitated mass-transfer in the more opened pore structure of the former material.

Summarizing the data, we could assume good catalytic activity for the supported well-crystallized and easily reducible spinel $Co_3O_4$ species. This assumption is not surprising taking into account the crucial role of oxygen release from the cobalt oxide lattice for ethyl acetate oxidation *via* the Mars van Krevelen mechanism [93]. The optimal size of these particles and their homogeneous distribution in the porous support seems to be of primary importance for the catalytic activity, and their formation is facilitated in the case of supports with larger mesopores. The pore size influences the process of the formation of these cobalt oxide particles, but this effect seems to also be affected by the topology of the pore structure. As a whole, the silicas with larger pores facilitate the mass-transfer during the samples preparation procedure, and thus, leads to more homogeneous distribution of cobalt oxide particles inside the pore system. However, the particle growth seems to be facilitated for the 3D structures with interpenetrating- (KIT-6) or cage-like (KIT-5) pores, and much less pronounced for the 2-D arranged straight pores of SBA-15 matrix. Moreover, here again, the more open pore structure could facilitate the catalytic process due to enhanced mass-transfer.

## 4. Conclusions

$Co_3O_4$ species with different dispersion can be prepared by wet impregnation of large pore ordered mesoporous silicas with cobalt nitrate. Spinel $Co_3O_4$ species exhibit higher reducibility and better catalytic activity in comparison with small amorphous particles strongly interacting with the support. Their formation is facilitated for silicas with larger mesopores, which are generally obtained after aging at higher temperatures. The effect of the pore size is less pronounced for the SBA-15 materials, where the straight cylindrical pores with 2-D arrangement probably leads to homogeneous distribution of the loaded cobalt oxide particles along the pore surface. For the 3D structures with interpenetrated cylindrical mesopores (KIT-6) or cage-like mesopores (KIT-5), the formation of homogeneously dispersed spinel $Co_3O_4$ species seems to be facilitated in mesoporous silicas with pores larger than 6 nm. However, mass-transfer effects also seem to influence the catalytic activity, as the catalytic activity of Co/KIT-6 materials are generally lower than that observed for the Co/SBA-15 and Co/KIT-5 materials.

## Acknowledgements

Financial support of Bulgarian-Finland fund and NSF, Ministry of Education and Science (project BY-X-305/07) is gratefully

acknowledged. We also acknowledge Dr. Sami Areva for the XPS spectra, Dr. Momtchil Dimitrov for the cobalt samples preparation and Prof. Christo Minchev for the support.

## Appendix A. Supplementary data

Supplementary data associated with this article can be found, in the online version, at doi:10.1016/j.apcatb.2008.12.015.

## References

[1] R.B. Anderson, The Fischer-Tropsch Synthesis, Academic Press, 1984.
[2] E. Iglesia, Appl. Catal. A: General 161 (1997) 59–78.
[3] B.H. Davis, Top. Catal. 32 (2005) 143–168.
[4] S.L. Soled, E. Iglesia, R.A. Fiato, J.E. Baumgartner, H. Vroman, S. Miseo, Top. Catal. 26 (2003) 101–109.
[5] M. Shelef, Chem. Rev. 95 (1995) 209–225.
[6] B. Wichterlova, Top. Catal. 28 (2004) 131–140.
[7] L.I. Simandi, Kluwer Academic Publishers, Dordrecht, 1992, p. 1.
[8] S. Vetrivel, A. Pandurangam, J. Mol. Catal. A: Chem. 227 (2005) 269–278.
[9] S. Bessell, Appl. Catal. A General 126 (1995) 235–244.
[10] R.J. Farrauto, C.H. Bartholomew, Fundamental of Industrial Catalytic Processes, Blackie Academic and Professional, London, 1997, 640–644.
[11] J. Spivey, J. Butt, Catal. Today 11 (1992) 465–500.
[12] T.V. Choudhary, S. Banerjee, V.R. Choudhary, Appl. Catal. A General 234 (2002) 1–24.
[13] M. Labaki, S. Siffert, J.-F. Lamonier, E.A. Zhilinskaya, A. Aboukais, Appl. Catal. B Environ. 43 (2003) 261–271.
[14] J.G. McCarthy, Y.-F. Chang, V.L. Wong, M.E. Johansson, Div. Petrol. Chem. 42 (1997) 158–165.
[15] F. Grillo, M.M. Natile, A. Glisenti, Appl. Catal. B: Environ. 48 (2004) 267–274.
[16] M. Che, B. Canosa, A.R. Gonzalez-Elipe, J. Chem. Soc. Faraday Trans. 78 (1982) 1043–1050.
[17] Y.J. Mergler, J. Hoebink, B.E. Nieuwenhuys, J. Catal. 167 (1999) 305–313.
[18] R.C. Reuel, C.H. Bartholomew, J. Catal. 85 (1984) 78–88.
[19] M. Voss, D. Borgmann, G. Wedler, J. Catal. 212 (2002) 10–21.
[20] K. Bourikas, C. Kordulis, J. Vakros, A. Lycourghiotis, Adv. Coll. Int. Sci. 110 (2004) 97–120.
[21] H. Li, S. Wang, F. Ling, J. Li, J. Mol. Cat. A: Chem. 244 (2006) 33–40.
[22] A.Y. Khodakov, A. Griboval-Constant, R. Bechara, F. Villain, J. Phys. Chem. B 105 (2001) 9805–9811.
[23] A.Y. Khodakov, V.L. Zholobenko, R. Bechara, D. Durand, Microporous Mesoporous Mater. 79 (2005) 29–39.
[24] A. Martínez, C. López, F. Márquez, I. Díaz, J. Catal. 220 (2003) 486–499.
[25] D. Yin, W. Li, W. Yang, H. Xiang, Y. Sun, B. Zhong, S. Peng, Microporous Mesoporous Mater. 47 (2001) 15–24.
[26] J. Panpranot, J.G. Goodwin Jr., A. Sayari, Catal. Today 77 (2002) 269–284.
[27] Y. Wang, M. Noguchi, Y. Takahashi, Y. Ohtsuka, Catal. Today 68 (2001) 3–9.
[28] A.Y. Khodakov, A. Griboval-Constant, R. Bechara, V.L. Zholobenko, J. Catal. 206 (2002) 230–241.
[29] T. Vrålstad, W.R. Glomm, M. Rønning, H. Dathe, A. Jentys, J.A. Lercher, G. Øye, M. Stocker, J. Sjoblom, J. Phys. Chem. B 110 (2006) 5386–5394.
[30] A. Taguchi, F. Schüth, Microporous Mesoporous Mater. 77 (2005) 1–45.
[31] T. Tsoncheva, J. Rosenholm, C.V. Teixeira, M. Dimitrov, M. Linden, C. Minchev, Microporous Mesoporous Mater. 89 (2006) 209–218.
[32] T. Tsoncheva, J. Rosenholm, M. Linden, L. Ivanova, C. Minchev, Appl. Catal. A: General 318 (2007) 234–243.
[33] T. Tsoncheva, Tz. Venkov, M. Dimitrov, C. Minchev, K. Hadjiivanov, J. Molec. Catal. A: Chem. 209 (2003) 125–134.
[34] R. Köhn, D. Paneva, M. Dimitrov, T. Tsoncheva, I. Mitov, C. Minchev, M. Fröba, Microporous Mesoporous Mater. 63 (2003) 125–137.
[35] T. Tsoncheva, J. Rosenholm, M. Lindén, F. Kleitz, M. Tiemann, L. Ivanova, M. Dimitrov, D. Paneva, I. Mitov, C. Minchev: Microporou Mesoporous Mater. doi:10.1016/j.micromeso.2007.10.005.
[36] T. Tsoncheva, S. Areva, M. Dimitrov, D. Paneva, I. Mitov, M. Linden, C. Minchev, J. Mol. Catal. A: Chem. 246 (2006) 118–127.
[37] J. Shi, Z. Hua, L. Zhang, Mater. Chem. 14 (2004) 795–806.
[38] S. Förster, Top. Cur. Chem. 226 (2003) 1–28.
[39] D.Y. Zhao, Q.S. Huo, J.L. Feng, B.F. Chmelka, G.D. Stucky, Chem. Mater. 120 (2000) 6024–6036.
[40] P.L. Ravikovitch, A.V. Neimark, J. Phys. Chem. B 105 (2001) 6817–6823.
[41] M. Kruk, M. Jaroniec, C.H. Ko, R. Ryoo, Chem. Mater. 12 (2000) 1961–1968.
[42] R. Ryoo, C.H. Ko, M. Kruk, V. Antochsuk, M. Jaroniec, J. Phys. Chem. B 104 (2000) 11465–11471.
[43] M. Kruk, V. Antochshuk, J.R. Matos, L.P. Mercuri, M. Jaroniec, JACS 124 (2002) 768–769.
[44] T.W. Kim, R. Ryoo, M. Kruk, K.P. Gierzal, M. Jaroniec, S. Kamiya, O. Terassaki, J. Phys. Chem. B 108 (2004) 11480–11489.
[45] J.R. Matos, M. Kruk, L.P. Mercuri, M. Jaroniec, L. Zhao, T. Kamiyama, O. Terasaki, T.J. Pinavia, Y. Liu, J. Am. Chem. Soc. 125 (2003) 821–829.
[46] M. Choi, W. Heo, F. Kleitz, R. Ryoo, Chem. Commun. (2003) 1340–1341.
[47] F. Kleitz, S.H. Choi, R. Ryoo, Chem. Commun. (2003) 2136–2137.
[48] F. Kleitz, T.W. Kim, R. Ryoo, Langmuir 22 (2006) 440–445.
[49] F. Kleitz, D. Liu, G.M. Anilkumar, I.S. Park, L.A. Solovyov, A.N. Shmakov, R. Ryoo, J. Phys. Chem. B 107 (2003) 14296–14300.
[50] J. Fan, C. Yu, F. Gao, J. Lei, B. Tian, L. Wang, Q. Luo, B. Tu, W. Zhou, D. Zhao, Angew. Chem. Int. Ed. 42 (2003) 3146–3150.
[51] H.J. Shin, R. Ryoo, M. Kruk, M. Jaroniec, Chem. Commun. (2001) 349–350.
[52] K. Flodström, V. Alfredsson, Microporous Mesoporous Mater. 59 (2003) 167–176.
[53] F. Kleitz, T. Czuryszkiewicz, L.A. Solovyov, M. Lindén, Chem. Mater. 18 (2006) 5070–5079.
[54] A.Y. Khodakov, V.L. Zholobenko, R. Bechara, D. Durand, Microporous and Mesoporous Mater. 79 (2005) 29–39.
[55] A. Jentys, N.H. Pham, H. Vinek, M. Englisch, J.A. Lercher, Catal. Today 39 (1998) 311–315.
[56] A. Jentys, N.H. Pham, H. Vinek, M. Englisch, J.A. Lercher, Microporous Mater. 6 (1996) 13–17.
[57] J. Panpranot, J.G. Goodwin, A. Sayari, J. Catal. 211 (2002) 530–539.
[58] T. Vråstad, G. Øye, M. Stöker, J. Sjöblom, Microporous Mesoporous Mater. 104 (2007) 10–17.
[59] S. Suvanto, T.A. Pakkanen, J. Mol. Catal. A: Chem. 164 (2000) 273–280.
[60] Y. Ohtsuka, Y. Takahashi, M. Noguchi, T. Arai, S. Takasaki, N. Tsubouchi, Y. Wang, Catal. Today 89 (2004) 419–429.
[61] A.Y. Khodakov, R. Bechara, A. Griboval-Constant, Appl. Catal. A: General 254 (2003) 273–288.
[62] A.Y. Khodakov, J. Lynch, D. Bazin, B. Rebours, N. Zanier, B. Moisson, P. Chaumette, J. Catal. 168 (1997) 16–25.
[63] D.G. Castner, Ph.R. Watson, I.Y. Chan, J. Phys. Chem. 93 (1989) 3188–3194.
[64] S.-W. Ho, J. Catal. 175 (1998) 139–151.
[65] A. Martinez, G. Prieto, J. Catal. 245 (2007) 470–476.
[66] X. Liu, B. Tian, C. Yu, F. Gao, S. Xie, B. Tu, R. Che, L.-M. Peng, D. Zhao, Angew. Chem. Int. Ed. 41 (2002) 3876–3878.
[67] K. Flodström, V. Alfredsson, N. Källrot, J. Am. Chem. Soc. 125 (2003) 4402–4403.
[68] P.O. Larsson, A. Andersson, J. Catal. 179 (1998) 72–89.
[69] A.R. Gandhe, J.S. Rebello, J.L. Figueiredo, J.B. Fernandes, Appl. Catal. B: Environ. 72 (2007) 129–135.
[70] L. Gasnot, V. Decottignies, J.F. Pauwels, Fuel 84 (2005) 505–518.
[71] B. Marler, U. Oberhagemann, S. Vortmann, H. Gies, Microporous Mater. 6 (1996) 375–383.
[72] P.I. Ravikovitch, A.V. Neimark, Langmuir 18 (2002) 9830–9837.
[73] J. Gallardo, A. Duran, D. Di Martino, R.M. Almeida, J. Non-Cryst. Solids 298 (2002) 219–225.
[74] X. Feng, G.E. Fryxell, L.Q. Wang, A.Y. Kim, J. Liu, K.M. Kemner, Science 276 (1997) 923–926.
[75] M.S. Ghattas, Microporous Mesoporous Mater. 97 (2006) 107–113.
[76] F.F. Bently, L.D. Smithson, A.L. Rozek, Wiley, New York, 1968, p. 1516.
[77] M.A. Camblor, A. Corma, J.P. Pariente, J. Chem. Soc. Chem. Commun. (1993) 557–559.
[78] P. Innocenzi, J. Non-Cryst. Solids 316 (2003) 309–319.
[79] M. Cerruti, G. Magnacca, V. Bolis, C. Morterra, J. Mater. Chem. 13 (2003) 1279–1286.
[80] K. Kojima, H. Taguchi, J. Matsuda, J. Phys. Chem. 95 (1991) 7595–7598.
[81] N. Martyanov, S. Uma, S. Rodrigues, K.J. Klabunde, Langmuir 21 (2005) 2273–2280.
[82] G.A.H. Mekhemer, H.M.M. Abd-Allah, S.A.A. Mansour, Coll. Surf. A: Phys. Eng. Aspects 160 (1999) 251–259.
[83] Y. Okamoto, K. Nagata, T. Adachi, T. Imanaka, K. Inamura, T. Takyu, J. Phys. Chem. 95 (1995) 310–319.
[84] T. Ataloglou, C. Fountzoula, K. Bourikas, J. Vakros, A. Lycourghiotis, Ch. Kordulis, Applied Catal. A: General 288 (2005) 1–9.
[85] J. YangYan, M.C. Kung, W.M.H. Sachtler, H.H. Kung, J. Catal. 172 (1997) 178–186.
[86] J.-S. Girardon, E. Quinet, A. Griboval-Constant, P.A. Chernavskii, L. Gengembre, A.Y. Khodakov, J. Catal. 248 (2007) 143–157.
[87] J. George, S. Shylesh, A.P. Singh, Appl. Catal. A: General 290 (2005) 148–158.
[88] S. Bessell, Appl. Catal. A: General 96 (1993) 253–268.
[89] H.F.J. van't Blik, D.C. Koningsberger, R. Prins, J. Catal. 97 (1986) 210–218.
[90] G. Jacobs, Y. Ji, B.H. Davis, D. Cronauer, A.J. Kropf, C.L. Marshall, Appl. Catal. A: General 333 (2007) 177–191.
[91] L.B. Backman, A. Rautiainen, M. Lindblad, O. Jylhä, A.O.I. Krause, Appl. Catal. A: General 208 (2001) 223–234.
[92] E.L. Rodrigues, J.M.C. Bueno, Appl. Catal. A: General 232 (2002) 147–158.
[93] I.E. Wachs, Catal. Today 100 (2005) 79–94.